nature catalysis

ARTICLES

https://doi.org/10.1038/s41929-020-0454-9

Check for updates

Fungal-derived brevianamide assembly by a stereoselective semipinacolase

Ying Ye[1,12], Lei Du[2,3,12], Xingwang Zhang[2,4], Sean A. Newmister[1], Morgan McCauley[5], Juan V. Alegre-Requena[5], Wei Zhang[2], Shuai Mu[6], Atsushi Minami[7], Amy E. Fraley[1], Maria L. Adrover-Castellano[1], Nolan A. Carney[1], Vikram V. Shende[1], Feifei Qi[3], Hideaki Oikawa[7], Hikaru Kato[8], Sachiko Tsukamoto[8], Robert S. Paton[5,9], Robert M. Williams[5,10] ✉, David H. Sherman[1,11] ✉ and Shengying Li[2,3,4] ✉

Fungal bicyclo[2.2.2]diazaoctane indole alkaloids represent an important family of natural products with a wide spectrum of biological activities. Although biomimetic total syntheses of representative compounds have been reported, the details of their biogenesis, especially the mechanisms for the assembly of diastereomerically distinct and enantiomerically antipodal metabolites, have remained largely uncharacterized. Brevianamide A represents a basic form of the subfamily bearing a dioxopiperazine core and a rare 3-spiro-ψ-indoxyl skeleton. In this study, we have identified the brevianamide A biosynthetic gene cluster from *Penicillium brevicompactum* NRRL 864 and elucidated the metabolic pathway. BvnE was revealed to be an essential isomerase/semipinacolase that specifies the selective production of the natural product. Structural elucidation, molecular modelling and mutational analysis of BvnE as well as quantum chemical calculations have provided mechanistic insights into the diastereoselective formation of the 3-spiro-ψ-indoxyl moiety in brevianamide A. This occurs through a BvnE-controlled semipinacol rearrangement and a subsequent spontaneous intramolecular [4+2] hetero-Diels–Alder cycloaddition.

Fungal indole alkaloids bearing the unusual bicyclo[2.2.2] diazaoctane core have drawn considerable attention from natural product, synthetic and biological chemists for decades. A wealth of studies on the discovery of analogues (including semi-synthetic, synthetic and natural) and their biological activities and biosynthetic mechanisms have been conducted[1]. The prominent representatives of this structural family have been recognized by our laboratories and others as belonging to two main biogenetic subfamilies (Extended Data Fig. 1). The first subfamily, the dioxopiperazines, includes the insecticidal brevianamides A and B (**BA** and **BB**) from *Penicillium brevicompactum*[2], the anticancer agents (−)-notoamide A, isolated from *Aspergillus protuberus* (formerly *Aspergillus* sp. MF297-2), and (+)-notoamide A, from *Aspergillus amoenus* (formerly *Aspergillus versicolor* NRRL 35600), the anticancer agents stephacidins A and B from *Aspergillus ochraceus*, the sclerotiamides, versicolamides, taichunamides, antifungal waikialoids, amoenamide B, speramides and asperochramides. The second subfamily are the monooxopiperazines, which include the antiparasitic paraherquamides from *Penicillium* spp., the asperparalines, marcfortines, calmodulin-inhibiting malbrancheamides, chrysogenamide, mangrovamides, penioxalamine, penicimutamides and asperversiamides[1,3,4].

The bicyclo[2.2.2]diazaoctane core structure has long been proposed to arise from an intramolecular [4+2] hetero-Diels–Alder (IMDA) construction[5–10]. In our continuing pursuit of biocatalysts responsible for the [4+2] cycloaddition reaction that is essential for the assembly of diverse diastereomerically distinct and enantiomerically antipodal metabolites, we realized that dioxopiperazines and monooxopiperazines have distinct biosynthetic strategies for building their respective bicyclo[2.2.2]diazaoctane scaffold (Fig. 1a). For instance, we recently revealed that the bifunctional NADPH-dependent reductase/Diels–Alderase MalC (and PhqE) catalyses diastereo- and enantioselective IMDA cyclization via a zwitterionic intermediate for the assembly of the monooxopiperazines malbrancheamides (and paraherquamides)[11]. However, the biosynthetic gene clusters for dioxopiperazines such as notoamides lack a MalC/PhqE homologue (Extended Data Fig. 2), indicating alternative yet uncharacterized mechanisms for the generation of their bicyclo[2.2.2]diazaoctane system.

BA and **BB** are among the original natural alkaloids isolated that comprise the bicyclo[2.2.2]diazaoctane core (Fig. 1a)[2]. After we established the correct absolute configuration of natural (+)-**BB** through total synthesis[12,13], it became evident that the biogenesis of **BA** and **BB** must accommodate the assembly of the core pseudo-enantiomeric tricyclic ring systems. Based on the pioneering proposal first suggested by Porter and Sammes in 1970 (ref. [14]), several hypotheses for their biogenesis were proposed to accommodate the stereochemistry, presumably installed by a [4+2]

[1]Life Sciences Institute, University of Michigan, Ann Arbor, MI, USA. [2]State Key Laboratory of Microbial Technology, Shandong University, Qingdao, China. [3]Shandong Provincial Key Laboratory of Synthetic Biology, CAS Key Laboratory of Biofuels, Qingdao Institute of Bioenergy and Bioprocess Technology, Chinese Academy of Sciences, Qingdao, China. [4]Laboratory for Marine Biology and Biotechnology, Qingdao National Laboratory for Marine Science and Technology, Qingdao, China. [5]Department of Chemistry, Colorado State University, Fort Collins, CO, USA. [6]Tianjin Institute of Pharmaceutical Research, Tianjin, China. [7]Department of Chemistry, Faculty of Science, Hokkaido University, Sapporo, Japan. [8]Graduate School of Pharmaceutical Sciences, Kumamoto University, Kumamoto, Japan. [9]Chemical Research Laboratory, University of Oxford, Oxford, UK. [10]University of Colorado Cancer Center, Aurora, CO, USA. [11]Departments of Medicinal Chemistry, Chemistry and Microbiology & Immunology, University of Michigan, Ann Arbor, MI, USA. [12]These authors contributed equally: Ying Ye, Lei Du. ✉e-mail: robert.williams@colostate.edu; davidhs@umich.edu; lishengying@sdu.edu.cn

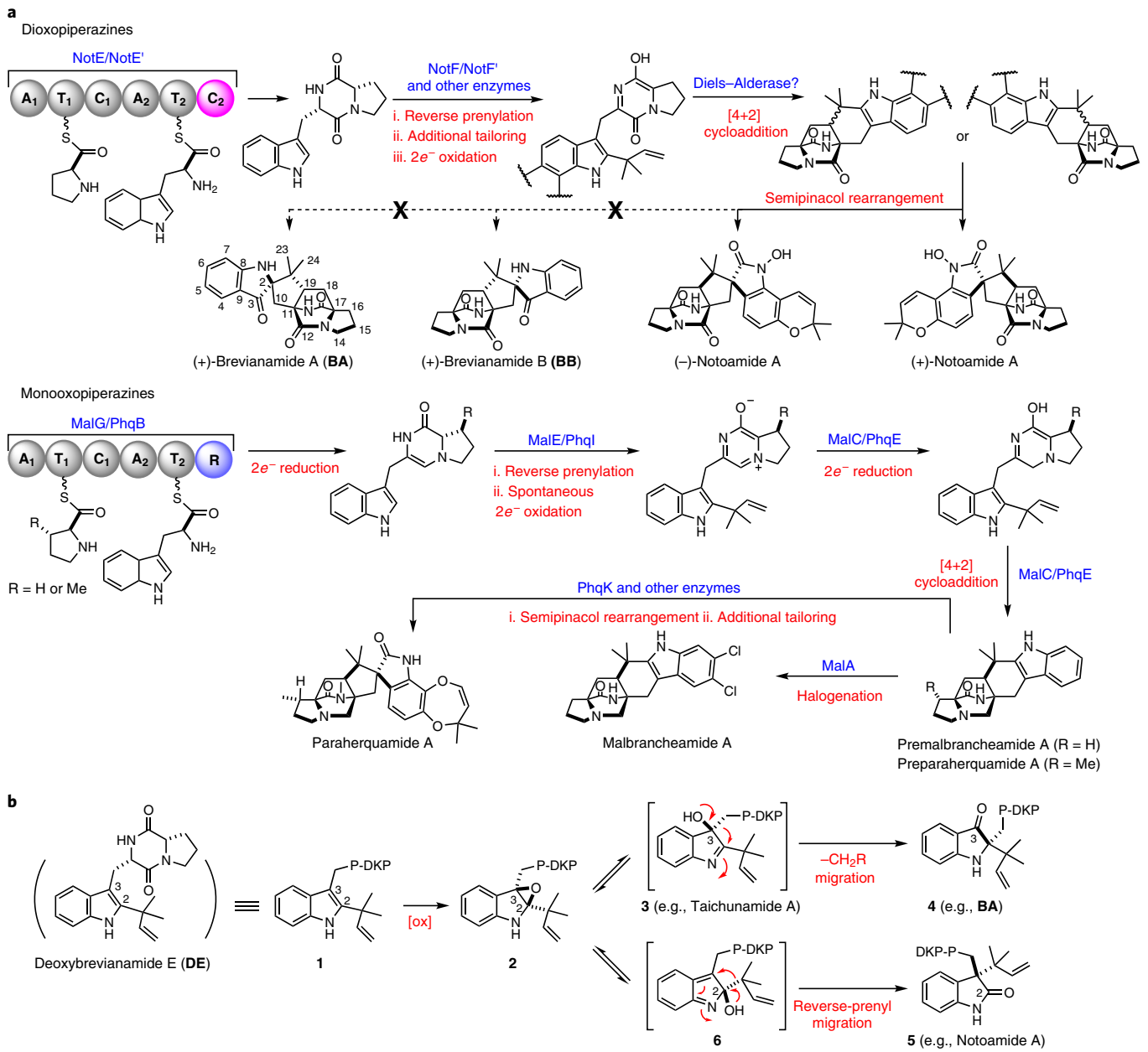

Fig. 1 | Present knowledge on bicyclo[2.2.2]diazaoctane assembly and semipinacol rearrangements of indole 2,3-epoxide systems. a, Distinct biosynthetic strategies for the assembly of the bicyclo[2.2.2]diazaoctane core structure in dioxopiperazines and monooxopiperazines. **b**, Disparate fates of the indole 2,3-epoxide (**2**) and semipinacol rearrangements leading to a stable 3-hydroxyindolenine (**3**), an indoxyl (**4**) and an oxindole (**5**). P-DKP refers to the prolyl-dioxopiperazine moiety of **DE**. Diketopiperazine and dioxopiperazine are synonymous terms.

IMDA cycloaddition, and the unique 3-spiro-ψ–indoxyl moiety. Specifically (Fig. 1b and Extended Data Fig. 3), a highly modified, reverse-prenylated indole (**1**, for example, deoxybrevianamide E (**DE**)) undergoes an apparent indole 2,3-epoxidation either before or after the IMDA cyclization. Ring-opening of epoxide **2** can form the 3-hydroxyindolenine (**3**), which in some instances is stable (for example, taichunamide A; ref. [15]) or suffers a spontaneous semipinacol rearrangement to ultimately generate a 3-spiro-ψ-indoxyl (via intermediate **4**, for example, **BA**), or a spiro-2-oxindole (via intermediate **5**, for example, notoamide A; ref. [16]) via an alternative ring-opening intermediate **6** (refs. [1,3,4]).

Although spiro-2-oxindoles are frequently observed in the prenylated indole alkaloid family, only a small number of 3-spiro-ψ-indoxyl species have been isolated so far, and very rarely are natural spiro-2-oxindoles and 3-spiro-ψ-indoxyls co-produced by a single microbe[17,18]. These co-metabolite profiles suggest that the semipinacol rearrangement might be differentially controlled in the partitioning of the putative indole 2,3-epoxides and implies a specific biocatalyst-controlled mechanism. Recently, the chemical synthesis of **BA**, a structure that contains both the dioxopiperazine and 3-spiro-ψ-indoxyl moieties, was accomplished and suggested a Diels–Alderase-free biosynthesis[19]. However, the biocatalytic details and sequential timing for the putative indole oxidation, semipinacol rearrangement and IMDA cycloaddition (Extended Data Fig. 3) remain unresolved experimentally due to the lack of access to the key enzymes.

In this study, we have addressed these outstanding biosynthetic questions by elucidating the **BA** biosynthetic pathway through gene disruption, heterologous expression, precursor incorporation experiments and in vitro biochemical analysis. In particular, an

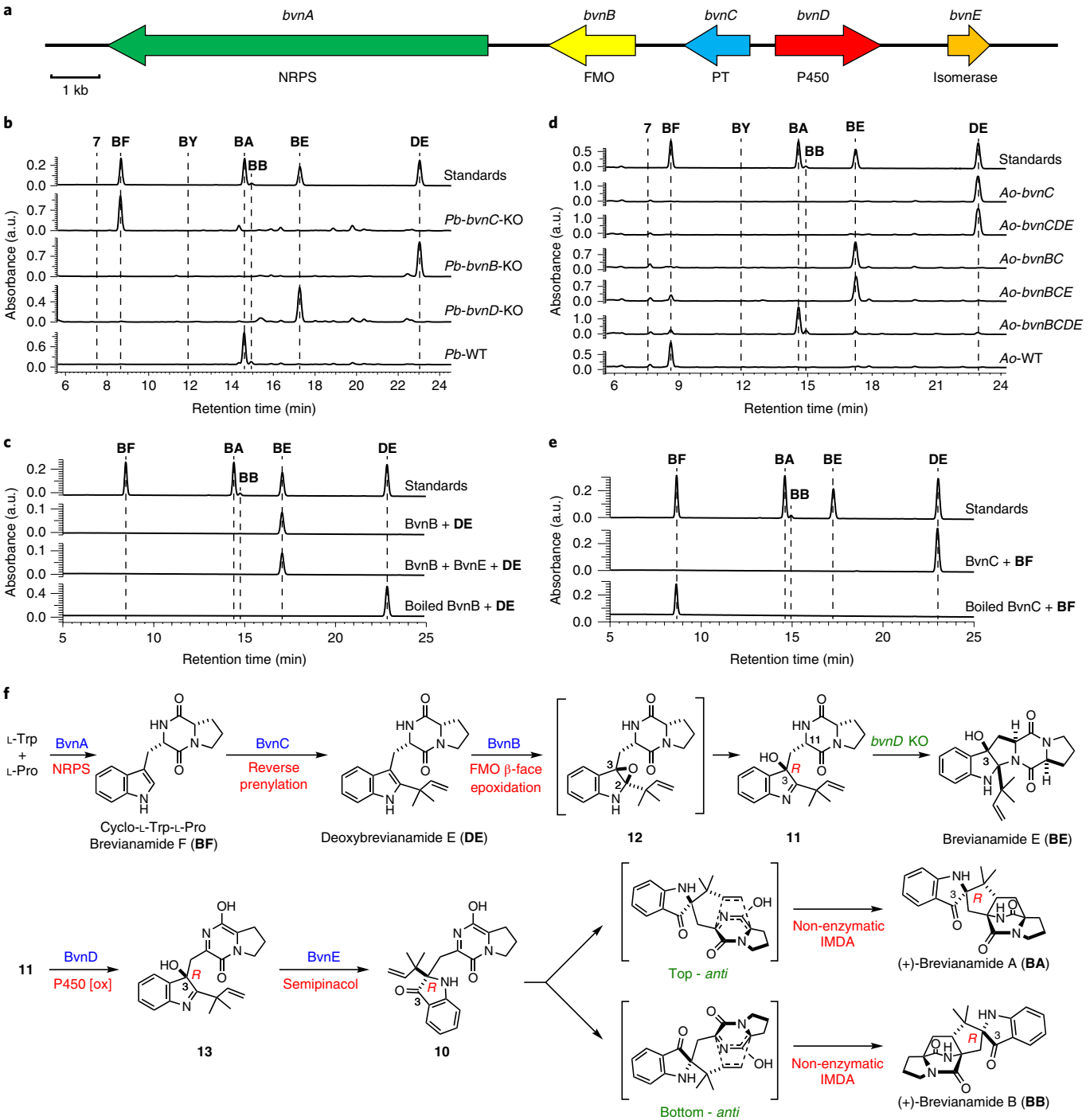

Fig. 2 | Functional analysis of brevianamide A biosynthetic genes and the proposed biosynthetic pathway. a, Brevianamide A biosynthetic gene cluster (*bvn*) from *P. brevicompactum* NRRL 864. **b**, HPLC analysis (230 nm) of *Pb* KO mutants. **c**, HPLC analysis (230 nm) of the in vitro assays of BvnB and BvnE. **d**, HPLC analysis (230 nm) of the brevianamide F (**BF**) feeding experiments with recombinant *A. oryzae* NSAR1 (*Ao*) strains expressing different *bvn* gene(s). **e**, HPLC analysis (230 nm) of in vitro assays using BvnC. **f**. Revised biosynthetic pathway for **BA** and **BB**.

isomerase/semipinacolase BvnE was revealed to catalyse an essential semipinacol rearrangement, thereby directing the diastereoselective assembly of **BA** by a spontaneous [4+2] IMDA cycloaddition reaction. Resolution of this 50-year-old mechanistic mystery together with our recent characterization of the Diels–Alderase-mediated biogenesis of monooxopiperazines[11] highlight the diversified biosynthetic strategies deployed by fungi for creating structurally diverse spiro-cyclized indole alkaloids.

Results and discussion

Identification of the brevianamide A biosynthetic gene cluster. Initially, genome mining of **BA**-producing strain *P. brevicompactum* NRRL 864 (*Pb*) was conducted using the notoamide non-ribosomal peptide synthetase (NRPS) gene *notE* as a probe to search for its homologue responsible for assembling the cyclodipeptide brevianamide F (**BF**)[3]. A putative 16-kilobase (kb) **BA** biosynthetic gene cluster (*bvn*, GenBank accession number: MN401751) was revealed

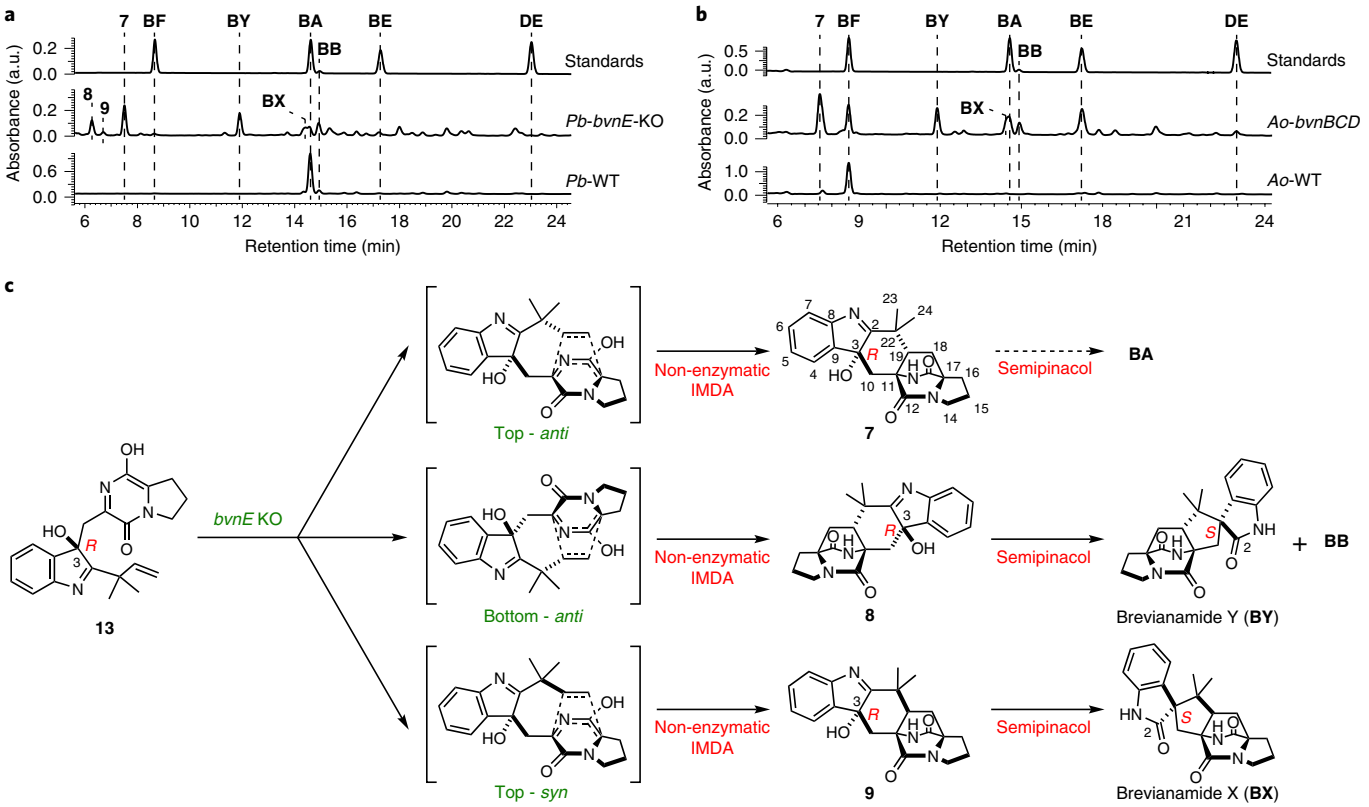

Fig. 3 | Functional analyses of *bvnE*. **a**, HPLC analysis (230 nm) of the *Pb-bvnE*-KO mutant. **b**, HPLC analysis (230 nm) of the **BF** feeding experiment of the *Ao-bvnBCD* mutant. **c**, The putative spontaneous transformations in the absence of BvnE.

(Fig. 2a) that contains *bvnA* (NRPS), *bvnB* (flavin monooxygenase, FMO), *bvnC* (prenyltransferase, PT) and *bvnD* (cytochrome P450 monooxygenase, P450), all of which have homologues in the (+)-/(−)-notoamide A biosynthetic gene clusters[3]. The *bvnE* gene (465 bp) that encodes a putative isomerase shows low homology to Trt14, AusH and PrhC involved in meroterpenoid biosynthetic pathways[20]. Interestingly, the biosynthetic gene clusters of the spiro-2-oxindole-containing notoamides and paraherquamides[3] lack a *bvnE* homologue (Extended Data Fig. 2), and further mining of these corresponding genomes failed to identify homologous genes. Thus, we surmised that BvnE might play an important role in 3-spiro-ψ-indoxyl formation.

Functional analysis of brevianamide A biosynthetic genes. In the *bvn* gene cluster, the bimodular NRPS encoded by *bvnA* is predicted to catalyse **BF** formation. This was confirmed by its heterologous expression in *Aspergillus oryzae* NSAR1 (*Ao*; Supplementary Fig. 1). To investigate the functions of *bvnB*–*E*, four individual single gene knockout (KO) strains of *Pb* were constructed. The resulting *Pb-bvnC*-KO strain accumulated **BF** (Fig. 2b) as the only product. The *Pb-bvnB*-KO and *Pb-bvnD*-KO strains accumulated **DE** and brevianamide E (**BE**; Fig. 2b), respectively. **BE** is proposed to be a rearranged shunt product resulting from the initial 2,3-indole epoxidation of **DE** by BvnB FMO (Fig. 2f). Indeed, the recombinant *N*-hexahistidine-tagged BvnB efficiently converted **DE** into **BE** in vitro (Fig. 2c), likely through a mechanism previously demonstrated for NotB (a BvnB homologue with 62%/75% identity/similarity) in notoamide biosynthesis[21]. Because *Pb-bvnD*-KO did not produce a bicyclo[2.2.2]diazaoctane structure, we reasoned that BvnD is a key enzyme for the proposed IMDA reactions.

When *bvnE* was deleted from *Pb*, five detectable substances were observed in addition to low levels of **BA** (Supplementary Table 1 and Supplementary Figs. 2 and 3) and **BB** (Fig. 3a), all showing the same molecular weight of 365 Da (Supplementary Fig. 4). These include three previously unknown 3-hydroxyindolenine derivatives **7**–**9** and the two reported spiro-2-oxindoles brevianamide X (**BX**) and brevianamide Y (**BY**). The planar structure of **7** was constructed on the basis of one- and two-dimensional NMR analyses (Supplementary Table 2 and Supplementary Figs. 5–10): the key heteronuclear multiple bond correlations (HMBCs) of C23/24-H_3 to C2/19/22, C10-H_2 to C2/3/11/19 and H4 to C3 (Supplementary Fig. 9) readily pointed to the hexatomic ring neighbouring the indole base, the C2=N double bond was deduced from the chemical shift of C2 (189.29 ppm) and the α-configuration of 3-OH was determined from a nuclear Overhauser effect spectroscopy (NOESY) analysis (Supplementary Fig. 10). The absolute configuration of **7** was determined by comparison of the experimental and computational electronic circular dichroism (ECD) spectra (Extended Data Fig. 4). The structures of **BX** and **BY** were determined by high-resolution mass spectrometry (Supplementary Fig. 4), NMR analyses (Supplementary Table 1 and Supplementary Figs. 11–22) and comparison with the corresponding synthesized authentic standards (see Supplementary Methods). Their absolute configurations were established by single-crystal X-ray diffraction analysis (CCDC nos. 1973959 (**BX**) and 1973957 (**BY**); Extended Data Fig. 4 and Supplementary Table 3). The ratio of **BA**/**BB**/**7**/**BX**/**BY** was determined to be 1:1:7:5:9 (Supplementary Table 4). The instability of **8** and **9** prevented direct structural determination of these isomers. Nonetheless, the observations that **8** quickly collapsed to **BY** and **BB** and **9** collapsed to **BX** (Supplementary Fig. 23), as well as their similar UV spectra to that of **7**, suggested the structures of these two unstable metabolites were 3-hydroxyindolenines (Fig. 3c and Supplementary Fig. 24). To determine the structures of **8** and **9**, we chemically synthesized their hypothetical structures (see Supplementary Methods and

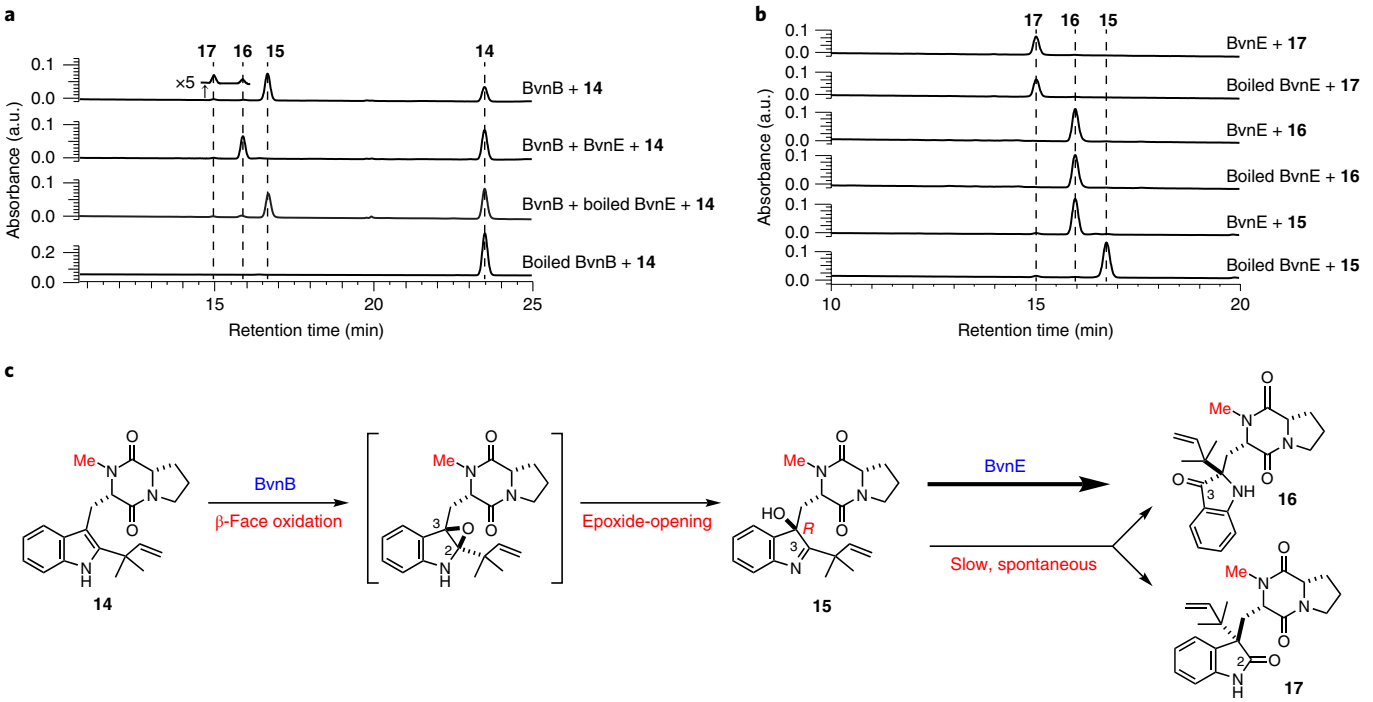

Fig. 4 | Probing the functionality of BvnE using substrate mimics. a, HPLC analysis (230 nm) of the in vitro assays of BvnB and BvnE. **b**, HPLC analysis (230 nm) of the in vitro assays of BvnE with the *N*-methylated substrates. **c**, The reaction scheme.

Supplementary Figs. 25–28). The matching UV spectra and HPLC retention times, as well as the same decomposition behaviour of the synthetic standards as the isolated samples (Supplementary Fig. 29), confirmed their structures.

To validate the function of *bvn* genes and also to clarify the order of biosynthetic steps, we conducted heterologous expression with different gene combinations in *Ao*. As expected, **BF** was converted into **DE** by either *Ao-bvnC* in vivo (Fig. 2d) or purified BvnC in vitro in the presence of dimethylallyl pyrophosphate (DMAPP) and Mg^{2+} (Fig. 2e). Thus, PT BvnC is a deoxybrevianamide E synthase, as previously demonstrated for NotF[22]. *Ao-bvnCDE* produced **DE** exclusively in the feeding experiment, whereas *Ao-bvnBC* and *Ao-bvnBCE* both accumulated **BE** exclusively (Fig. 2d). These results indicate that the presumed indole epoxidation catalysed by BvnB FMO occurs prior to the P450 BvnD-mediated step and preceding the BvnE-catalysed step. Upon the introduction of **BF** to the *Ao-bvnBCD* culture, five products with identical $m/z = 366$ ($[M+H]^+$) were observed (Fig. 3b and Supplementary Fig. 4). Their relative abundance (**BA**/**BB**/**7**/**BX**/**BY** = 1:1:5:2:6) was qualitatively consistent with the observations for *Pb-bvnE*-KO (Fig. 3a and Supplementary Table 4) except that derivatives **8** and **9** were not detected, probably due to their instability. Finally, when *bvnE* was incorporated and the *Ao-bvnBCDE* strain grown in the presence of exogenous **BF**, we observed **BA** and **BB** in a ratio of ~10:1 (Fig. 2d and Supplementary Table 4), which is consistent with the product profile of wild-type *Pb* (*Pb*-WT; Fig. 2b).

These results demonstrated that the metabolites generated through *Ao* biotransformations and individual *Pb* knockout mutants correlated directly with one another. The reaction sequence of each enzyme in the pathway can now be deduced as BvnA→BvnC→BvnB→BvnD→BvnE (Fig. 2f). Both systems showed a BvnE-dependent change of product profile, suggesting that BvnE might function to mediate the formation of the 3-oxo species **10**, and directly impact the diastereo-outcome of the presumed IMDA reactions. With respect to BvnD activity, intensive attempts to produce this P450 enzyme in *Escherichia coli* and *Saccharomyces cerevisiae* were unsuccessful, thus preventing direct functional analysis. Nonetheless, the results showing that *Ao-bvnBCD* transformed **BF** into multiple IMDA products (Fig. 3b) and that *Ao-bvnCDE* was unable to recognize **DE** as a substrate (Fig. 2d), along with the principles for P450 enzymes and Diels–Alder reactions, together suggest that BvnD might oxidize non-isolable intermediate **11** (derived from ring-opening of the indole epoxide **12**) to **13**, thereby generating the diene moiety required for IMDA cyclization (Fig. 2f). In the absence of BvnD, compound **11** would collapse to **BE** through an energetically favoured N–C ring closure (Supplementary Fig. 30).

Although we cannot exclude the possibility that BvnD might directly desaturate the N–C bond in the dioxopiperazine ring of **11** (ref. [23]), it is more likely that BvnD first catalyses the hydroxylation of **11** and then undergoes spontaneous dehydration/tautomerization to yield **13** (Fig. 2f). Regarding the position on **11** likely oxidized by BvnD, bond dissociation energy calculations (Supplementary Fig. 31) indicated that the most probable hydroxylation site is the tertiary C–H bond at C11, which is supported by the following two facts: firstly, FtmG, a BvnD homologue with 47%/64% protein sequence identity/similarity in the fumitremorgin biosynthetic pathway, has been experimentally confirmed to catalyse the hydroxylation of an analogous position[23] and secondly, the fungal dioxopiperazine structure asperversiamide I was recently discovered to contain a hydroxylated C11, which might have been installed by an unidentified BvnD homologue[24].

Probing the catalytic mechanism of the isomerase/pinacolase BvnE. Based on the results obtained with *Pb-bvnE*-KO and *Ao-bvnBCD* (Fig. 3), BvnE appears to be a central enzyme for controlling the product profile in brevianamide biogenesis. To assess this unique isomerase in vitro, the *N*-hexahistidine-tagged BvnE was produced in *E. coli* BL21(DE3) and purified to homogeneity (Supplementary Fig. 32). Next, we sought to identify the potential natural substrate of BvnE from *Pb-bvnE*-KO. Compounds **7**–**9**, **BX**, **BY** and **BE** were tested as substrates, but failed to be transformed (Supplementary

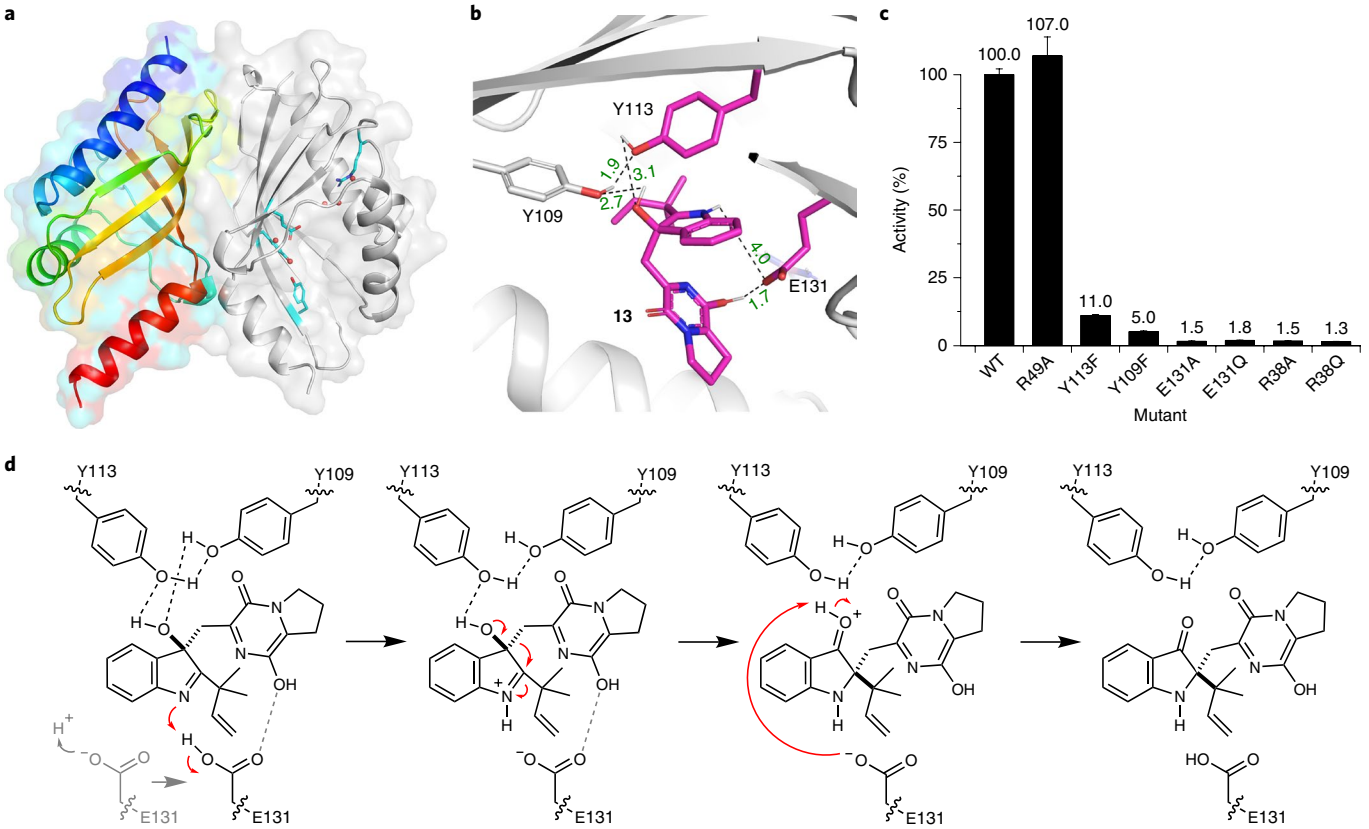

Fig. 5 | BvnE crystal structure, docking and the proposed catalytic mechanism. a, Structural overview of BvnE: the left chain shows in rainbow colours the N terminus (blue) to the C terminus (red), and the right chain in grey cartoon representation shows putative catalytic acid/basic residues (cyan) and water molecules in the active site (red spheres). **b**, The docked BvnE–**13** complex with the key residues, and hydrogen bonding distances shown in Å. **c**, Site-directed mutagenesis results. The data represent the average of independent experiments performed in triplicate (central values represent means, error bars represent standard deviations and $n = 3$). **d**, The proposed reaction mechanism for the isomerization of **13** catalysed by BvnE. Glu131-mediated proton transfer could be assisted by Arg38, which interacts with Glu131 through an ordered water network (Extended Data Fig. 6c). Indirect deprotonation of the oxonium intermediate via bound solvent molecules rather than a direct interaction with Glu131 cannot be excluded.

Figs. 33 and 34). Thus, we hypothesized that **13** might be the native substrate of BvnE. Considering the inaccessibility of this unstable intermediate, we elected to chemoenzymatically synthesize **15** (see Supplementary Methods), a stable analogue of **13** (Fig. 4c), to block the dioxopiperazine nitrogen from N–C ring closure and prevent the formation of the unstable azadiene intermediate upon spontaneous dehydration. The mechanistic probe **15** was prepared through BvnB-catalysed in vitro conversion of the chemically synthesized *N*-methyl-deoxybrevianamide E (**14**; Supplementary Figs. 35–43), and the absolute configuration of **15** was determined by single-crystal X-ray diffraction analysis (CCDC no. 1973958; Extended Data Fig. 4). Interestingly, two minor products, **16** and **17**, were also generated from **14** along with the predominant product **15** (Fig. 4a). Structural determination indicated that **16** and **17** are 3-oxo and 2-oxo isomers of **15**, respectively (Supplementary Table 5 and Supplementary Figs. 35 and 44–55). Their absolute configurations were determined by comparison of their experimental and calculated ECD spectra (Extended Data Fig. 4), which were consistent with the structures arising from the semipinacol rearrangement of **15**. Moreover, when **15** was incubated with BvnE, it was completely converted into **16** (Fig. 4b). These results indicate that BvnE functions as a semipinacolase responsible for the selective formation of the 3-spiro-ψ-indoxyl substructure (in **16**) from the 3-hydroxypyrrole moiety (in **15**). The spontaneous conversion of **15** into **16** and **17** at room temperature could also occur slowly (Fig. 4c and Supplementary Fig. 56). Loss of stereocontrol of the IMDA cycloaddition reaction in terms of top/bottom (**7**/**9**/**BA**/**BX** vs **8**/**BY**/**BB**) and *anti*/*syn* selectivity (**7**/**8**/**BA**/**BB**/**BY** vs **9**/**BX**) in the absence of BvnE strongly suggests that these isomers are generated from non-enzymatic IMDA reactions. Moreover, the observed product profile (Fig. 3 and Supplementary Table 6) is quantitatively consistent with the calculated product distribution (see below). With respect to the catalytic properties of BvnE (Extended Data Fig. 5), the apparent k_{cat} and K_m values of BvnE towards **15** were determined to be 0.013 min^{-1} and 822 μM, respectively, under the optimal pH (6.5) and temperature (30 °C). The low catalytic efficiency ($k_{cat}/K_m = 1.58 \times 10^{-5}\,min^{-1}\,\mu M^{-1}$) is probably because **15** is not the native substrate.

As a key component in controlling product outcome in brevianamide biosynthesis, we sought to determine how BvnE catalyses the formation of the 3-spiro-ψ-indoxyl species. BvnE is related to the NTF2-like superfamily enzymes that have been studied in fungal meroterpenoid biogenesis[20]. We solved the crystal structure of BvnE at 1.8 Å resolution (Fig. 5a and Supplementary Table 7; Protein Data Bank (PDB) ID: 6U9I) by molecular replacement using PrhC (PDB ID: 5X9J) as search model[25] (Supplementary Fig. 57). BvnE is a symmetric homodimer that adopts an α+β-barrel fold with the presumed active sites at the end of each barrel. This cavity has a hydrophobic interior and also contains several polar residues that could be involved in the acid/base chemistry reported for this family of enzymes (Fig. 5a and Supplementary Fig. 58).

Docking of the presumed native substrate **13** (Fig. 5b and Extended Data Fig. 6a) helped to reveal the BvnE active site.

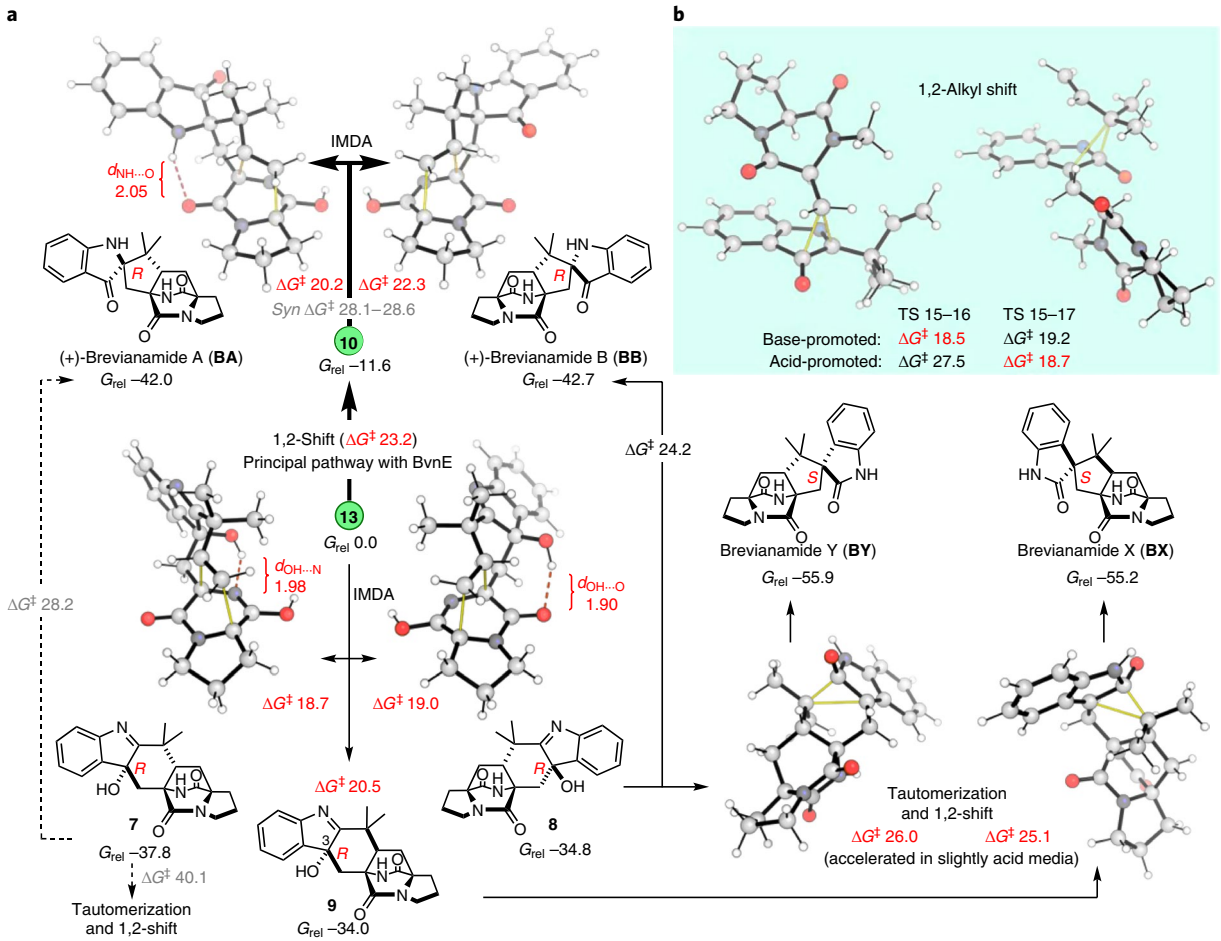

Fig. 6 | Results of the quantum chemical calculations. a, The *anti*-selective IMDA transition-state structures and products accessible from intermediates **13** and **10**. **b**, The 1,2-alkyl shift (semipinacol) transition-state structures for the migration of CH_2-dioxopiperazine (left) and reverse-prenyl (right) groups. The computed Gibbs energies are given in kcal mol^{-1} and the highlighted distances in Å. Normal lines represent the major pathways obtained under *Pb-bvnE*-KO conditions. Pathways in bold correspond to the major reaction obtained when using BvnE (switch in reactivity). Dashed lines represent pathways with prohibitively high activation energies under the reaction conditions.

We identified Arg38, Tyr109, Tyr113 and Glu131 as candidates for site-directed mutagenesis and in vitro enzyme assays with **15**. In each case, mutation of these residues caused severely attenuated activity (Fig. 5c). All the CD spectra of the BvnE mutants matched the wild-type protein (Extended Data Fig. 6b), indicating that these point mutations did not significantly impact protein folding. The electron density data indicate that Arg38, Tyr113 and Glu131 adopt multiple conformations in the BvnE crystal lattice. Therefore, these residues were designated as flexible in molecular docking (Extended Data Fig. 6c). In the lowest-energy output of the BvnE–**13** docking complex, the reverse-prenyl group of the substrate is packed into a hydrophobic pocket (Extended Data Fig. 6a), and Tyr109 and Tyr113 interact with the 3-OH of **13** (Fig. 5b). Glu131 is positioned to interact with the indole nitrogen and the C18 oxygen of **13**, suggesting its key role in the semipinacol rearrangement (Fig. 5d). On the basis of these docking studies, we propose that the reaction mechanism involving BvnE includes Glu131-mediated proton transfer to initiate the semipinacol rearrangement and provide charge stabilization of the intermediate, and hydrogen-bond-assisted activation of the semipinacol rearrangement through Tyr109/Try113 (Fig. 5d). Arg38, which is essential for activity, does not directly interact with the docked ligands or active site residues. However, the structure reveals two ordered water molecules in a hydrogen-bonding network between Arg38 and Glu131 (Extended Data Fig. 6c), suggesting that it may assist in proton transfer by regenerating the carboxylate form of E131.

Quantum chemical calculations. Next, we used density functional theory and coupled cluster theory calculations (SMD-DLPNO-CCSD(T)/cc-pV(DT)Z//M06-2X-D3/6-31+G(d,p); see Supplementary Methods) to evaluate the intermediate and transition-state (TS) structures in the revised brevianamide biosynthetic pathway (Figs. 2f and 3c), and to explore the innate regio- and stereochemical preferences associated with the key steps (Fig. 6a). Accordingly, under *Pb-bvnE*-KO conditions, the IMDA reactions that transform **13** into **7**–**9** are favoured. In the calculated mechanism, only two diastereomers of **7** (**8** and **9**) undergo a subsequent 1,2-alkyl shift to irreversibly generate **BY** and **BB** (from **8**) and **BX** (from **9**). Before the shifts that lead to the formation of the ring system, an initial tautomerization that switches the position of the OH group between C3 and C2 proceeds quickly (Supplementary Fig. 59). The reason **7** fails to undergo subsequent transformation is likely due to the high energy required for the tautomerization process (35.5 kcal mol^{-1} between **7** and its tautomer; Supplementary Fig. 60). In the computed kinetic profile, the initial irreversible IMDA (from **13** to **7**–**9**) and CH_2-dioxopiperazine shift (from **13** to **10**) determine the selectivity of the process and their activation barriers are consistent with room-temperature reactivity

over the course of minutes and hours. Considering that **BY** and **BX** are the major products obtained from **8** and **9**, respectively, the calculated results agree qualitatively with the experimental results: the two most favourable products are **7** and **BY**, followed by **BX**, with **BA** and **BB** being minor products (experimental ratio **BY**/**7**/**BX**/**BA**/**BB** = 9:7:5:1:1; Supplementary Table 4).

The semipinacol rearrangement to form 3-spiro-ψ-indoxyl **10** is favourably exergonic and irreversible ($\Delta G = -11.6\,kcal\,mol^{-1}$). Competition between the two possible non-enzymatic semipinacol rearrangements (CH_2-dioxopiperazine vs reverse-prenyl shifts) was found computationally to depend strongly on whether the reaction undergoes basic activation of the hydroxy group or acidic activation of the imine group (Fig. 6b): whereas general/specific acidic activation of the nitrogen results in a buildup of positive charge in the migrating group in the TS, favouring 1,2-prenyl migration ($\Delta\Delta G^{\ddagger} = 8.8\,kcal\,mol^{-1}$), basic activation of the hydroxy group has the opposite effect, inverting the selectivity to favour migration of the dioxopiperazine-containing group ($\Delta\Delta G^{\ddagger} = 0.7\,kcal\,mol^{-1}$). The contrast between the regioselective biocatalytic conversion of **13** into **10** and the spontaneous conversion of **15** into **16**/**17** under acid/base conditions corroborates the involvement of the hydrogen-bond acceptors Tyr113 or Tyr109 as a likely candidate for the activation of the 3-hydroxy group by BvnE (Fig. 5d and Supplementary Fig. 61) during this key step.

Next, we investigated the distinct IMDA cyclization reactions from **10** and **13** (Fig. 6a). In each case, there are four possible stereochemical outcomes. The selectivity for *anti* over *syn* cycloadducts is controlled by the balance between stabilizing intramolecular hydrogen bonds and unfavourable steric interactions (Supplementary Fig. 62). Whereas the *syn* pathways from **10** are highly disfavoured relative to the *anti* pathways, those from **13** form C–H···O interactions[26,27], making them more competitive (Supplementary Fig. 63). In this regard, the levels of IMDA diastereoselectivity of **10** are exceptional, displaying high selectivity for the formation of **BA** ($20.2\,kcal\,mol^{-1}$) over the pseudo-enantiomeric bicyclo[2.2.2]diazaoctane **BB** ($22.3\,kcal\,mol^{-1}$) due to an intramolecular N–H···O hydrogen bond, with a very large (~$6\,kcal\,mol^{-1}$) preference for the two *anti*-configured products (**BA** and **BB**) over their *syn* diastereomers (28.1–$28.6\,kcal\,mol^{-1}$) (Fig. 6a). The stereospecific conversion of **7** into **BA** through a ring contraction was found to be more challenging than the earlier 1,2-rearrangements (activation barrier of $28.2\,kcal\,mol^{-1}$); however, this process is exergonic by $4\,kcal\,mol^{-1}$. Accordingly, this ring contraction can be accomplished under laboratory conditions by treating **7** with sodium hydroxide in water (Fig. 3c and Supplementary Fig. 64).

Conclusions

We have characterized and fully reconstituted the biosynthesis of **BA** and **BB** and identified a key semipinacolase, BvnE, that mediates diastereocontrol for subsequent spontaneous [4+2] cycloaddition for the biogenesis of the brevianamides. The formation of the dioxopiperazine bicyclo[2.2.2]diazaoctane core construct has also been demonstrated and the computational data support a spontaneous [4+2] pericyclic reaction. Resolution of this mechanistic mystery together with our recent characterization of the Diels–Alderase-mediated biogenesis of monooxopiperazines[11] highlight the diversified biosynthetic strategies deployed by fungi for creating structurally diverse spiro-cyclized indole alkaloids. However, several important mechanistic questions remain, including what are the mechanistic details of the BvnD-catalysed two-electron oxidation required for azadiene formation to enable the IMDA reaction, and what, if any, biogenetic relationships exist between the brevianamides and other dioxopiperazine families comprising the bicyclo[2.2.2]diazaoctane system, such as (+)/(−)-notoamide A, whose producer genomes lack apparent *bvnE* homologues?

Note added in proof: During production of this Article the total synthesis of brevianamide A which supports a spontaneous intramolecular [4+2] Diels-Alder construction by R. C. Godfrey et al. was published[19].

Methods

Strains and culture conditions. All *E. coli* strains were grown at 37 °C unless otherwise specified. The *E. coli* DH5α strain was used for vector construction and plasmid isolation using Luria-Bertani (LB) agar plates or LB liquid media. The *E. coli* BL21(DE3) strain was used for protein production and purification, and cultured in Terrific Broth (TB: 1.2% tryptone, 2.4% yeast extract, 0.94% K_2HPO_3, 0.22% KH_2PO_3, 4% glycerol) media. *P. brevicompactum* NRRL 864 (*Pb*) was obtained from the Agricultural Research Service Culture Collection (NRRL) collection. *Pb* was cultured on potato dextrose agar (PDA) plates at 28 °C for 7 d before spore collection and preservation. For the fermentation of the brevianamides, solid Czapek–Dox agar (CDA) media were inoculated with the spore suspension and incubated at 28 °C for 6 d. *A. oryzae* NSAR1 (*Ao*) was a gift from Professor Oikawa's laboratory. *Ao* and its different transformants were grown on DPY (dextrin-polypeptone-yeast extract: 2% dextrin, 1% polypeptone, 0.5% yeast extract, 2% agar) agar plates at 30 °C for 7 d. For metabolite production, CMP liquid media (Czapek–Dox broth supplemented with 3% maltose and 1% peptone) were used. Upon inoculation, cultures were incubated at 28 °C for 5 d with shaking at 200 r.p.m. All the strains and vectors used in this study are listed in Supplementary Table 8.

Protein expression and purification of BvnB, BvnC and BvnE. For protein expression, the *E. coli* BL21(DE3) strain carrying a target gene expression plasmid was used. A single colony was picked, inoculated and cultured overnight at 37 °C in LB broth with appropriate selective antibiotics (commonly 50 μg ml^{-1} kanamycin unless otherwise specified). The overnight seed culture was inoculated (1:100) into 1 l TB medium containing 4% glycerol, selective antibiotics and 0.1% rare salt solution (0.68% $FeCl_3$, 0.05% $ZnCl_2$, 0.05% $CoCl_2$, 0.05% Na_2MoO_4, 0.025% $CaCl_2$, 0.047% $CuSO_4$, 0.013% H_3BO_3). The culture was then incubated at 37 °C with shaking at 220 r.p.m. Protein expression was induced by adding isopropyl-β-D-thiogalactoside (IPTG) to a final concentration of 0.2 mM, when the optical density at 600 nm (OD_{600}) reached ~0.6 (typically ~3 h after inoculation). The cells were grown for an additional 20 h at 18 °C at 220 r.p.m. After collecting the cells by centrifugation (4,000*g*, 15 min) at 4 °C, they were frozen at −20 °C for 30 min and then melted at ambient temperature. All protein purification procedures were conducted at 4 °C. Briefly, 40 ml lysis buffer (50 mM NaH_2PO_4, 300 mM NaCl, 10% glycerol, 5 mM imidazole, pH 7.5) was used to re-suspend the cell pellet by vortexing, and a Model 500 Sonic Dismembrator was used for ultrasonic cell lysis (5 s on, 5 s off, 1 h in total). After centrifugation at 12,000*g* for 30 min, the supernatant was collected, to which 1 ml nickel nitrilotriacetic acid (Ni-NTA) resin (Qiagen) was added and incubated on a shaker at 30 r.p.m. at 4 °C for 30 min. The slurry was then loaded onto an empty column. Then, 100–300 ml wash buffer (50 mM NaH_2PO_4, 300 mM NaCl, 10% glycerol, 10 mM imidazole, pH 7.5) was used to wash the protein-bound resin until no protein was detectable in flow-through in a Coomassie Brilliant Blue G-250 assay. Target proteins were eluted with 5 ml elution buffer (50 mM NaH_2PO_4, 300 mM NaCl, 10% glycerol, 250 mM imidazole, pH 7.5) and concentrated using an Amicon Ultra centrifugal filter with an appropriate molecular weight cutoff (Merck) at 5,000*g* for 30 min. The concentrated fraction (<1 ml) was loaded onto a PD-10 column (GE Healthcare) pre-equilibrated with 25 ml desalting buffer (50 mM NaH_2PO_4, 10% glycerol, pH 7.5) for buffer exchange. Aliquots of the desalted fraction (100 μl per tube) were flash-frozen using liquid N_2 and stored at −80 °C for later use.

Gene knockout in *Pb*. For targeted gene disruption in *Pb*, two specific homologous arms (~1 kb) were designed and amplified from *Pb* genomic DNA. Knockout vectors were constructed using common ligation or recombinase strategies, assembling the two arms respectively into the two multi-cloning sites (MCS) of the plasmid pRSF-hyg (Supplementary Fig. 65), which contains a hygromycin resistance marker for the selection of knockout mutants. The primers used in this study are listed in Supplementary Table 9. Gene knockout was performed using the split-marker strategy[28]. Briefly, two knockout cassette fragments were PCR-amplified using the primers x-up-F/Hyg-R (x indicates the target gene to be knocked out) and Hyg-F/x-down-R, and subsequently concentrated to >200 ng μl^{-1}. About 10 μl of each of the two concentrated samples were mixed and transformed into *Pb* protoplasts. The protoplast preparation and poly(ethylene glycol) (PEG)-mediated transformation were performed by following the procedures developed by Heneghan et al. with some minor modifications[29]. Specifically, PDA and potato dextrose broth were used as solid and liquid media, respectively. The protoplasts were collected immediately after lysing by enzyme digestion. The PEG-mediated protoplast transformation was conducted on PDA plates containing 1 M sorbitol and 100 μg ml^{-1} hygromycin as the selection antibiotic. The genotypes of the knockout mutants derived from homologous recombination were verified through PCR reaction with the appropriate primers listed in Supplementary Table 9.

Heterologous gene expression in *Ao*. A spore suspension of *Ao*-WT or an *Ao* mutant (1.0×10^6 cells) was inoculated into 100 ml DPY medium (2% dextrin, 1%

polypeptone, 0.5% yeast extract) supplemented with appropriate nutrients. After incubation for 3 d at 30 °C and 200 r.p.m., mycelia were collected by filtration and washed with double-deionized H_2O. Protoplasting was performed using Yatalase (Takara; 5.0 mg ml^{-1}) in Solution 1 (0.8 mM NaCl, 10 mM NaH_2PO_4, pH 6.0) at 30 °C for 2 h. The protoplasts were centrifuged at 900*g* (Beckman JLA10.500) for 5 min and washed with 0.8 M sterile NaCl solution. Then, the protoplasts were adjusted to 2.0×10^8 cells ml^{-1} by adding Solution 2 (0.8 M NaCl, 10 mM $CaCl_2$, 10 mM Tris-HCl, pH 8.0) and Solution 3 (40% (w/v) PEG4000, 50 mM $CaCl_2$, 50 mM Tris-HCl, pH 8.0) in a 4:1 volume ratio. The appropriate plasmid (13 µg) was added to the protoplast solution (200 µl). The aliquot was incubated on ice for 20 min, and then Solution 3 (1 ml) was added. After 20 min incubation at room temperature, Solution 2 (10 ml) was added to the mixture and the mixture was centrifuged at 900*g* (Beckman JLA10.500) for 5 min. The transformation mixture was poured onto CDA plates supplemented with 0.8 M NaCl and appropriate nutrients, and then overlaid with the soft-top agar (1.2 M sorbitol, 3.5% Czapek–Dox broth, 0.6% agar). The plates were incubated at 30 °C for 3–7 d until colonies showed up.

In vitro enzyme assays. Unless otherwise specified, all enzymatic assays were carried out in 100 µl of 50 mM Tris-HCl buffer (pH 7.5) at 30 °C for 2 h. The enzyme reaction mixture contained 1 mM substrate(s) (**BF** and DMAPP for BvnC, **DE** or **14** for BvnB, **15** for BvnE or its mutants), necessary cofactors (10 mM Mg^{2+} for BvnC, 2 mM NADPH for BvnB) and 10 µl of each purified enzyme.

Mutagenesis of BvnE. The mutagenesis PCR reaction was performed with 50 ng pET28b-*bvnE* as template, 0.2 µM primer (in our system, one primer is sufficient for successful mutagenesis), 2.5 µl 10× *Pfu* buffer, 0.5 µl dNTP mix (25 mM of each dNTP), 1 ml dimethyl sulfoxide and 0.5 µl *Pfu*Ultra II fusion HS DNA polymerase (Agilent) in a total volume of 25 µl. The PCR cycles were set as follows: (1) 95 °C for 3 min, (2) 95 °C for 30 s, (3) 53 °C for 1 min and (4) 65 °C for 2 min, with steps 2–4 repeated for 30 cycles. *Dpn*I digestion was performed with 1 µl of 2 U µl^{-1} *Dpn*I and 25 µl PCR reaction solution for 2 h at 37 °C. From the digested solution, 1 µl was used to transform 30 µl DH10β Electrocompetent Competent cells (Takara). The mutant plasmids were purified and subjected to sequencing at the University of Michigan DNA Sequencing Core.

BvnE protein expression and purification for crystallization. *E. coli* BL21(DE3)-pRARE2 was transformed with the plasmid (BvnE_pET28H8-MBP-T) and grown in 1 l TB medium with 50 µg ml^{-1} kanamycin and 100 µg ml^{-1} spectinomycin at 37 °C to $OD_{600} \approx 1$. The culture was cooled to 20 °C over 1 h, induced with 0.25 mM IPTG and incubated for 24 h (20 °C, 225 r.p.m. shaking). The cells were collected by centrifugation (4 °C, 5,000*g*) and stored at −20 °C. All BvnE purification steps were performed at 4 °C. The cell pellet was re-suspended in lysis buffer (50 mM Tris pH 7.5, 300 mM NaCl, 20 mM imidazole, 10 % glycerol, 0.5 mg ml^{-1} lysozyme, 0.05 mg ml^{-1} DNase, 5 mM $MgCl_2$) and lysed by sonication followed by high-speed centrifugation (4 °C, 60,000*g*, 25 min). The lysate was filtered (0.45 µm) and loaded onto a 5-ml Ni-NTA Histrap column of a fast protein liquid chromatograph (FPLC) and washed with 20 column volumes of Ni-NTA buffer (50 mM Tris pH 7.5, 300 mM NaCl, 20 mM imidazole, 10% glycerol) at 3 ml min^{-1}. BvnE was eluted with elution buffer (50 mM Tris pH 7.5, 300 mM NaCl, 500 mM imidazole, 10% glycerol). The pooled fractions were incubated with His-tagged tobacco etch virus (TEV) protease in a 1:20 molar ratio to remove the His-maltose binding protein (MBP) tag. The protein was dialysed overnight against 50 mM Tris pH 7.5, 300 mM NaCl and 2 mM dithiothreitol, and passed through a Ni-NTA column to remove TEV protease and MBP. Further purification was accomplished by size-exclusion chromatography using a Superdex 75 10/300 GL column equilibrated with 50 mM Tris pH 7.5 and 300 mM NaCl. SDS–PAGE was used to assess protein homogeneity; BvnE was determined to be >95% pure. The protein was concentrated using an Amicon Ultra centrifugal concentrator (10,000 nominal molecular weight limit) to 29 mg ml^{-1}. The concentration was determined by UV spectrophotometry using the calculated molar extinction coefficient.

Crystallization and structure determination. BvnE was screened for initial crystallization conditions using the Midwest Center Structural Genomics (MCSG) screen at 25 and 4 °C. Single, diffraction-quality crystals of BvnE were grown by the sitting drop vapour diffusion method at 4 °C by mixing 29 mg ml^{-1} BvnE with the well solution (26% PEG3350, 0.1 M Tris pH 8.5, 4% v/v pentaerythritol ethoxylate (3/4 EO/OH)) in a 1:1 ratio. Sitting droplets were nucleated from an earlier spontaneous crystallization using a cat whisker. Then, 8 µl of cryoprotectant (12.75% glycerol, 26% PEG3350, 0.1 M Tris pH 8.5, 4% v/v pentaerythritol ethoxylate (3/4 EO/OH), 50 mM Tris pH 7.5, 300 mM NaCl) was added directly to the sitting drops, and the crystals were collected using nylon loops and vitrified by rapid plunging into liquid nitrogen. Diffraction data were collected at beamline 23-ID-B at the Advanced Photon Source (APS) using an X-ray wavelength of 1.033 Å (360° of data, 0.2° image width, 100 K). The data were integrated and scaled with XDS[30]. The structure was solved by molecular replacement using PrhC (PDB ID: 5X9J) as search model (Phaser-MR)[31]. The final model was completed using alternate cycles of manual model building using Coot[32] and refinement using PHENIX.refine[33]. The structure was validated with MolProbity[34]. The data collection and refinement details are presented in Supplementary Table 7.

Molecular docking of BvnE with compound 13. Compound **13** was docked into the BvnE structure using the automated docking software Autodock4 (ref. [35]). The conformational heterogeneity of the key active site residues Arg38, Tyr113 and Glu131 experimentally observed in the electron density/crystal structure was incorporated into the docking model. Docking was performed with Arg38, Tyr113 and Glu131 as flexible residues in an effort to obtain the lowest-energy conformations.

Reporting Summary. Further information on research design is available in the Nature Research Reporting Summary linked to this article.

Data availability

The sequence data referenced in this study are available in GenBank with the accession number MN401751. Coordinates and associated structure factors have been deposited in the Protein Data Bank (PDB) with PDB ID 6U9I (BvnE) and in the Cambridge Crystallographic Data Centre (CCDC) with the CCDC numbers 1973959 (**BX**), 1973957 (**BY**) and 1973958 (**15**). Molecular coordinates as well as absolute and relative thermochemistry data have been provided for the computational studies. All other data are available from the corresponding authors on reasonable request.

Received: 5 October 2019; Accepted: 16 March 2020;
Published online: 18 May 2020

References

1. Klas, K. R. et al. Structural and stereochemical diversity in prenylated indole alkaloids containing the bicyclo[2.2.2]diazaoctane ring system from marine and terrestrial fungi. *Nat. Prod. Rep.* **35**, 532–558 (2018).
2. Birch, A. J. & Wright, J. J. The brevianamides: a new class of fungal alkaloid. *J. Chem. Soc. D* 644b–645b (1969).
3. Li, S. et al. Comparative analysis of the biosynthetic systems for fungal bicyclo[2.2.2]diazaoctane indole alkaloids: the (+)/(−)-notoamide, paraherquamide and malbrancheamide pathways. *MedChemComm* **3**, 987–996 (2012).
4. Finefield, J. M., Frisvad, J. C., Sherman, D. H. & Williams, R. M. Fungal origins of the bicyclo[2.2.2]diazaoctane ring system of prenylated indole alkaloids. *J. Nat. Prod.* **75**, 812–833 (2012).
5. Sanzcervera, J. F., Glinka, T. & Williams, R. M. Biosynthesis of the brevianamides: quest for a biosynthetic Diels–Alder cyclization. *J. Am. Chem. Soc.* **115**, 347–348 (1993).
6. Sanzcervera, J. F., Glinka, T. & Williams, R. M. Biosynthesis of brevianamides A and B: in search of the biosynthetic Diels–Alder construction. *Tetrahedron* **49**, 8471–8482 (1993).
7. Williams, R. M., Sanz-Cervera, J. F., Sancenon, F., Marco, J. A. & Halligan, K. Biomimetic Diels–Alder cyclizations for the construction of the brevianamide, paraherquamide sclerotamide, and VM55599 ring systems. *J. Am. Chem. Soc.* **120**, 1090–1091 (1998).
8. Adams, L. A., Valente, M. W. N. & Williams, R. M. A concise synthesis of *d*,*l*-brevianamide B via a biomimetically-inspired IMDA construction. *Tetrahedron* **62**, 5195–5200 (2006).
9. Williams, R. M. & Cox, R. J. Paraherquamides, brevianamides, and asperparalines: laboratory synthesis and biosynthesis. An interim report. *Acc. Chem. Res.* **36**, 127–139 (2003).
10. Stocking, E. M. & Williams, R. M. Chemistry and biology of biosynthetic Diels–Alder reactions. *Angew. Chem. Int. Ed.* **42**, 3078–3115 (2003).
11. Dan, Q. et al. Fungal indole alkaloid biogenesis through evolution of a bifunctional reductase/Diels–Alderase. *Nat. Chem.* **11**, 972–980 (2019).
12. Williams, R. M., Glinka, T. & Kwast, E. Facial selectivity of the intramolecular SN2′ cyclization: stereocontrolled total synthesis of brevianamide B. *J. Am. Chem. Soc.* **110**, 5927–5929 (1988).
13. Williams, R. M., Kwast, E., Coffman, H. & Glinka, T. Remarkable, enantio-divergent biogenesis of brevianamide A and B. *J. Am. Chem. Soc.* **111**, 3064–3065 (1989).
14. Porter, A. E. A. & Sammes, P. G. A Diels–Alder reaction of possible biosynthetic importance. *J. Chem. Soc. D* 1103a (1970).
15. Li, F. et al. Determination of taichunamide H and structural revision of taichunamide A. *Org. Lett.* **20**, 1138–1141 (2018).
16. Greshock, T. J. et al. Isolation, structure elucidation, and biomimetic total synthesis of versicolamide B, and the isolation of antipodal (−)-stephacidin A and (+)-notoamide B from *Aspergillus versicolor* NRRL 35600. *Angew. Chem. Int. Ed.* **47**, 3573–3577 (2008).
17. Kai, A., Kato, H., Sherman, D. H., Williams, R. M. & Tsukamoto, S. Isolation of a new indoxyl alkaloid, Amoenamide B, from *Aspergillus amoenus* NRRL 35600: biosynthetic implications and correction of the structure of Speramide B. *Tetrahedron Lett.* **59**, 4236–4240 (2018).
18. Xu, X., Zhang, X., Nong, X., Wang, J. & Qi, S. Brevianamides and mycophenolic acid derivatives from the deep-sea-derived fungus *Penicillium brevicompactum* DFFSCS025. *Mar. Drugs* **15**, 43 (2017).

19. Godfrey, R. C., Green, N. J., Nichol, G. S. & Lawrence, A. L. Total synthesis of brevianamide A. *Nat. Chem.* https://doi.org/10.1038/s41557-020-0442-3 (2020).
20. Mori, T. et al. Molecular basis for the unusual ring reconstruction in fungal meroterpenoid biogenesis. *Nat. Chem. Biol.* **13**, 1066–1073 (2017).
21. Li, S. et al. Biochemical characterization of NotB as an FAD-dependent oxidase in the biosynthesis of notoamide indole alkaloids. *J. Am. Chem. Soc.* **134**, 788–791 (2012).
22. Ding, Y. et al. Genome-based characterization of two prenylation steps in the assembly of the stephacidin and notoamide anticancer agents in a marine-derived *Aspergillus* sp. *J. Am. Chem. Soc.* **132**, 12733–12740 (2010).
23. Kato, N. et al. Identification of cytochrome P450s required for fumitremorgin biosynthesis in *Aspergillus fumigatus*. *ChemBioChem* **10**, 920–928 (2009).
24. Li, H. et al. HPLC–DAD-directed isolation of linearly fused prenylated indole alkaloids from a soil-derived *Aspergillus versicolor*. *J. Nat. Prod.* **82**, 2181–2188 (2019).
25. Matsuda, Y. et al. Discovery of key dioxygenases that diverged the paraherquonin and acetoxydehydroaustin pathways in *Penicillium brasilianum*. *J. Am. Chem. Soc.* **138**, 12671–12677 (2016).
26. Sutor, D. J. The C–H···O hydrogen bond in crystals. *Nature* **195**, 68–69 (1962).
27. Schwalbe, C. H. June Sutor and the C–H···O hydrogen bonding controversy. *Crystallogr. Rev.* **18**, 191–206 (2012).
28. Goswami, R. S. Targeted gene replacement in fungi using a split-marker approach. *Methods Mol. Biol.* **835**, 255–269 (2012).
29. Heneghan, M. N. et al. First heterologous reconstruction of a complete functional fungal biosynthetic multigene cluster. *ChemBioChem* **11**, 1508–1512 (2010).
30. Kabsch, W. XDS. *Acta Crystallogr. D* **66**, 125–132 (2010).
31. McCoy, A. J. et al. Phaser crystallographic software. *J. Appl. Crystallogr.* **40**, 658–674 (2007).
32. Emsley, P., Lohkamp, B., Scott, W. G. & Cowtan, K. Features and development of Coot. *Acta Crystallogr. D* **66**, 486–501 (2010).
33. Adams, P. D. et al. PHENIX: a comprehensive Python-based system for macromolecular structure solution. *Acta Crystallogr. D* **66**, 213–221 (2010).
34. Chen, V. B. et al. MolProbity: all-atom structure validation for macromolecular crystallography. *Acta Crystallogr. D* **66**, 12–21 (2010).
35. Morris, G. M. et al. AutoDock4 and AutoDockTools4: automated docking with selective receptor flexibility. *J. Comput. Chem.* **30**, 2785–2791 (2009).

Acknowledgements

This work was supported by the National Key Research and Development Program (2019YFA0905100 and 2019YFA0706900), the National Natural Science Foundation of China (21472204 and 31872729 to S.L. and 31800041 to L.D.), the National Institutes of Health R35 GM118101, the Hans W. Vahlteich Professorship (to D.H.S.), R01 CA070375 (to R.M.W. and D.H.S.), the Shandong Provincial Natural Science Foundation (ZR2019ZD20 to S.L. and ZR201807060986 to L.D.), the National Postdoctoral Innovative Talents Support Program (BX20180325 to L.D.), the China Postdoctoral Science Foundation (2019M652500 to L.D.) and funding from the NSF (grant no. CHE-0840456, for X-ray instrumentation). GM/CA@APS is supported by the National Institutes of Health, the National Institute of General Medical Sciences (AGM-12006) and the National Cancer Institute (ACB-12002). We thank J. L. Smith from the University of Michigan for her assistance with the structure determination of BvnE. R.S.P. acknowledges computational resources from the RMACC Summit supercomputer supported by the National Science Foundation (ACI-1532235 and ACI-1532236), the University of Colorado Boulder and Colorado State University, and the Extreme Science and Engineering Discovery Environment (XSEDE) through allocation TG-CHE180056. XSEDE is supported by the National Science Foundation (ACI-1548562). The authors thank X. Li and H. Sui from The State Key Laboratory of Microbial Technology, Shandong University for their assistance with single-crystal X-ray diffraction.

Author contributions

Y.Y., L.D., R.M.W., D.H.S. and S.L. contributed to the experimental design. Y.Y., L.D., W.Z. and F.Q. performed molecular cloning, fungal genetics and compound purification. Y.Y., L.D. and X.Z. performed structural assignment (NMR analysis). Y.Y., L.D., S.A.N., A.E.F. and M.L.A.-C. performed molecular cloning, protein expression and purification. Y.Y. and L.D. performed enzymatic assays, and LC–MS and HPLC analyses. S.A.N. and M.L.A.-C. carried out all crystallographic experiments and structural analyses. Y.Y. performed structure-based site-directed mutagenesis. W.Z. performed genome mining of the gene cluster. M.M., N.A.C., V.V.S. and S.M. synthesized and validated the compounds described in this study. J.V.A.-R and R.S.P. performed DFT calculations. A.M. and H.O. supplied the heterologous expression system. H.K. and S.T. performed ECD measurements and calculations. Y.Y., L.D., S.A.N., R.S.P., R.M.W., D.H.S. and S.L. analysed the data and prepared the manuscript.

Competing interests

The authors declare no competing interests.

Additional information

Extended data is available for this paper at https://doi.org/10.1038/s41929-020-0454-9.

Supplementary information is available for this paper at https://doi.org/10.1038/s41929-020-0454-9.

Correspondence and requests for materials should be addressed to R.M.W., D.H.S. or S.L.

Reprints and permissions information is available at www.nature.com/reprints.

Publisher's note Springer Nature remains neutral with regard to jurisdictional claims in published maps and institutional affiliations.

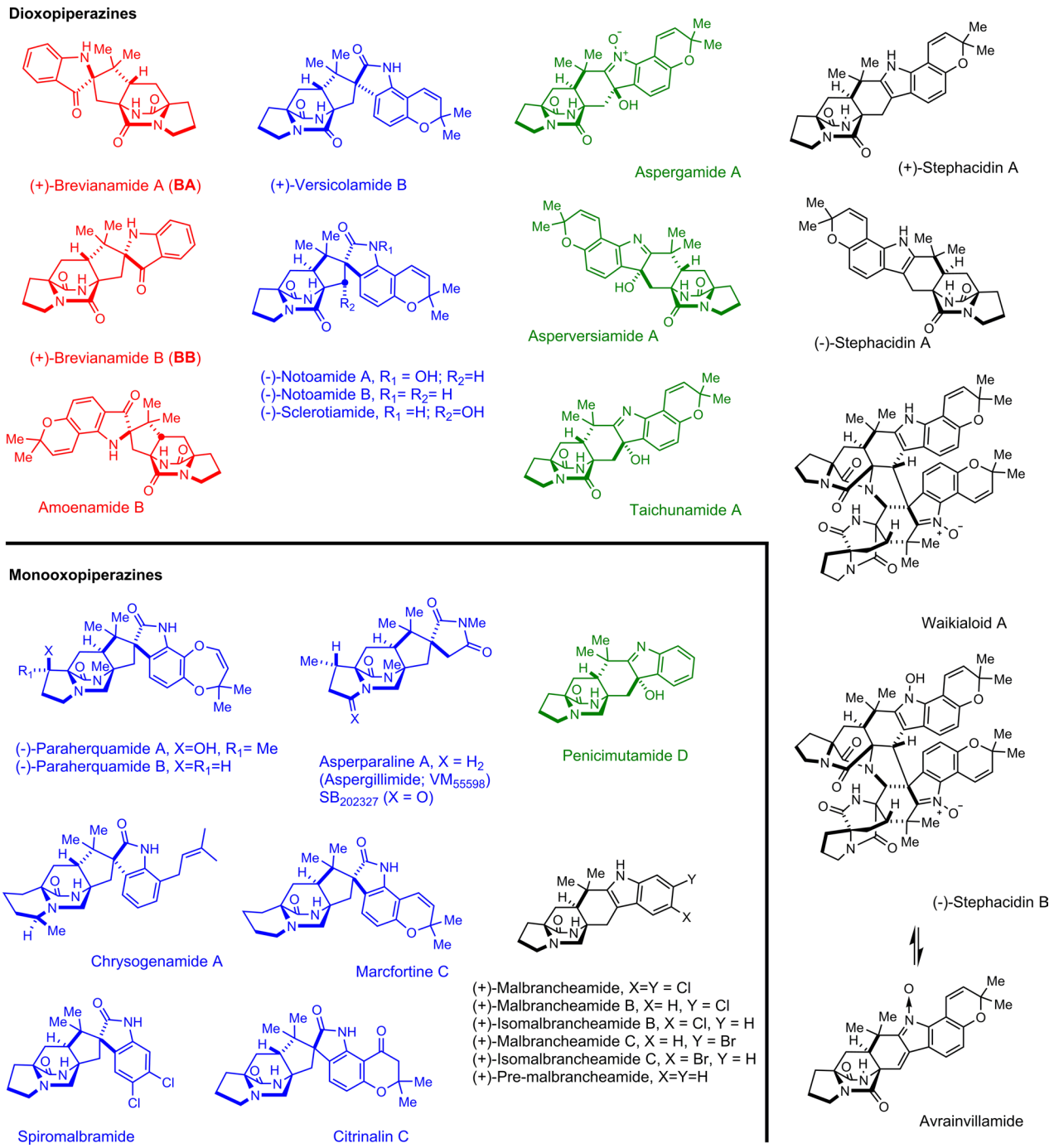

Extended Data Fig. 1 | Representative fungal bicyclo[2.2.2]diazaoctane indole alkaloids. Compounds with 3-*spiro*-ψ—indoxyls, *spiro*-2-oxindoles and 3-hydroxyindolenines are presented in red, blue and green, respectively.

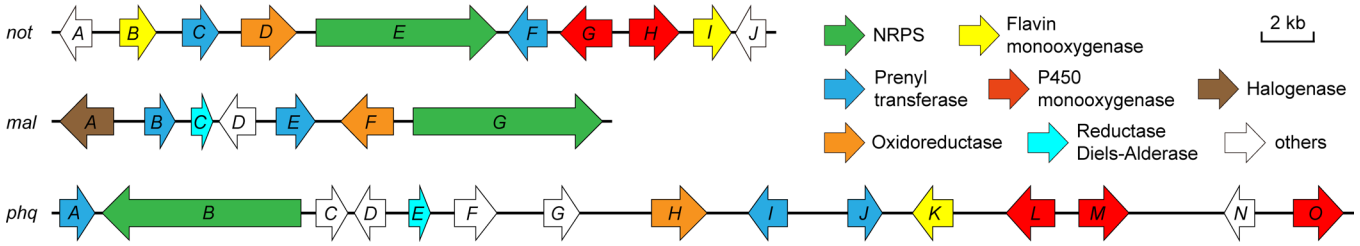

Extended Data Fig. 2 | The biosynthetic gene clusters for representative fungal bicyclo[2.2.2]indole alkaloids. The gene clusters *not*, *mal* and *phq* are responsible for biosynthesis of notoamides, malbrancheamides and parapherquamides, respectively.

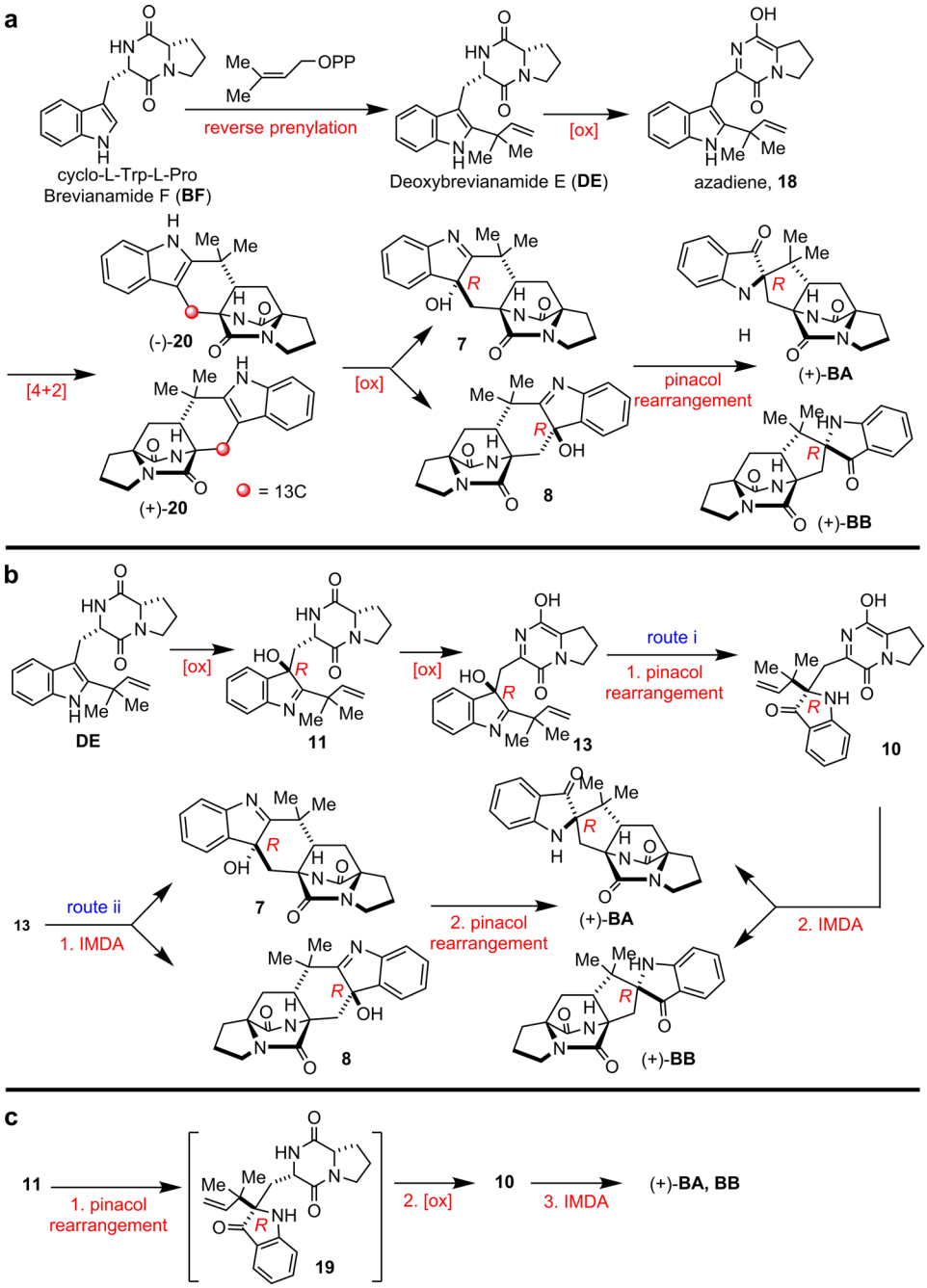

Extended Data Fig. 3 | Biogenetic proposals for Brevianamide A (BA) and Brevianamide B (BB). a, Early biosynthetic proposal suggested and interrogated by Williams *et. al*[13]. **b**, Original biogenesis proposed by Porter and Sammes (via **7**)[14]. **c**, More recent biosynthetic proposals suggested by Williams *et al.*[5,6,10]. Several biogenetic hypotheses based on the pioneering proposal first suggested by Porter and Sammes in 1970[14] reasoned that the bicyclo[2.2.2]diazaoctane core arises *via* an intramolecular [4+2] *hetero*-Diels-Alder (IMDA) construction[5–10,36]. We experimentally interrogated the biogenetic proposal **a**, through the synthesis of ^{13}C-labeled putative Diels-Alder products (±)-**20**, but could not detect incorporation into either **BA** or **BB** in cultures of *Pb*. Based on these results, we then suggested the biosynthetic pathways illustrated in **b** and **c**. The fundamental difference between the biogenesis described in **a**, and that in **b** and **c**, is the sequential timing of the indole oxidation, the semipinacol rearrangement and the crucial IMDA reactions. Thus, it remained conceivable that oxidation of **DE** to the (*R*)-hydroxyindolenine provides species **11**, which can suffer several fates. One is N-C ring closure to co-metabolite Brevianamide E (**BE**); a second possibility shown in **b** is oxidation and tautomerization to the azadiene species **13**, which can suffer IMDA cyclization providing **7** and **8**, then undergo a final semipinacol rearrangement to furnish **BA** and **BB** (*route i*). Alternatively, azadiene **13** could first suffer semipinacol rearrangement to **10**, which then undergoes the IMDA construction to generate **BA** and **BB** (*route ii*). Another possibility **c** involves (*R*)-hydroxyindolenine **11**, which proceeds through a semipinacol rearrangement to the indoxyl species **19**, followed by further oxidation to the azadiene species **10** and subsequent IMDA to furnish **BA** and **BB**. Experimental supports to distinguish between these proposed pathways, all of which embrace the relative and absolute stereochemistry of **BA** and **BB**, have remained unresolved until this work.

36. Williams, R. M., Sanz-Cervera, J. F., Sancenon, F., Marco, J. A. & Halligan, K. M. Biomimetic Diels–Alder cyclizations for the construction of the brevianamide, paraherquamide, sclerotamide, asperparaline and VM55599 ring systems. *Biorg. Med. Chem.* **6**, 1233–1241 (1998).

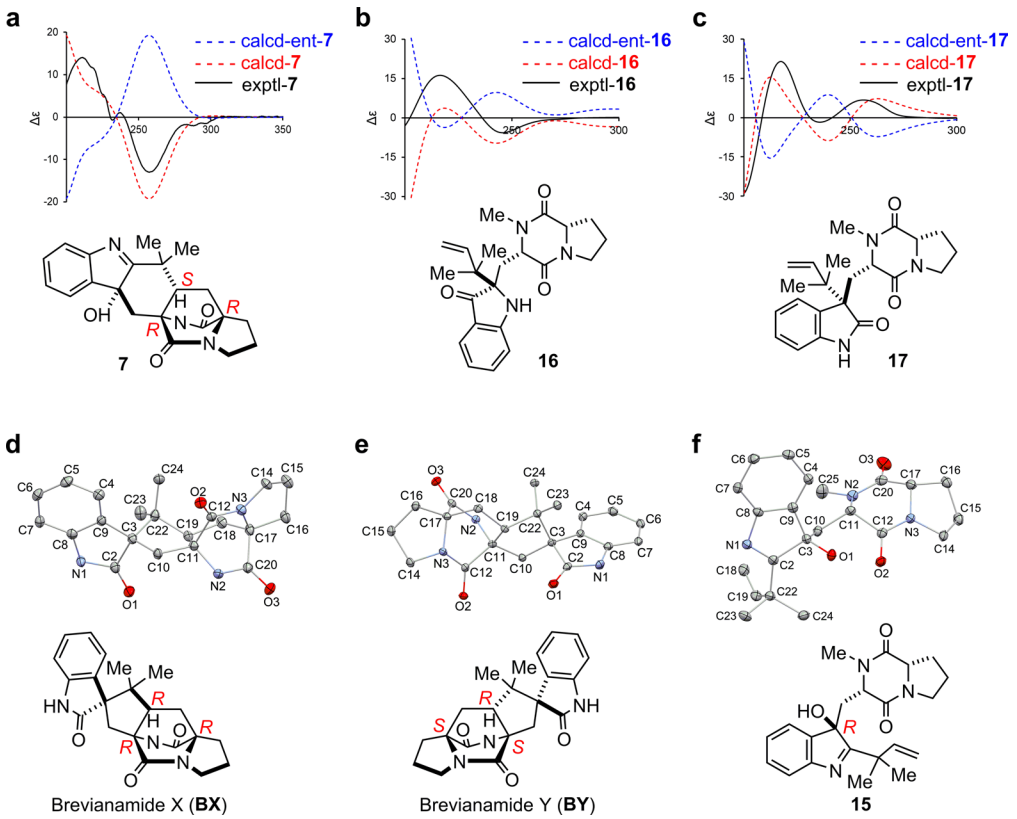

Extended Data Fig. 4 | Elucidation of absolute configurations. a, Experimental and computational CD spectra of **7**. **b**, Experimental and computational CD spectra of **16**. **c**, Experimental and computational CD spectra of **17**. **d**, X-ray ORTEP diagram of **BX**. **e**, X-ray ORTEP diagram of **BY**. **f**, X-ray ORTEP diagram of **15**.

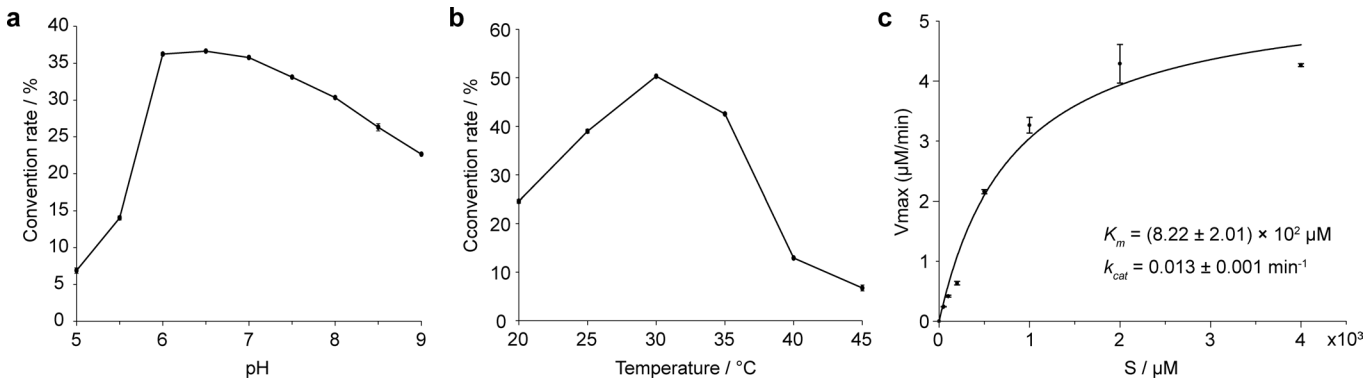

Extended Data Fig. 5 | Enzyme properties of BvnE using compound 15 as a substrate. a, pH dependency. **b**, temperature dependency. **c**, Michaelis-Menton kinetic analysis (centre values, means; error bars, standard deviations; n = 2).

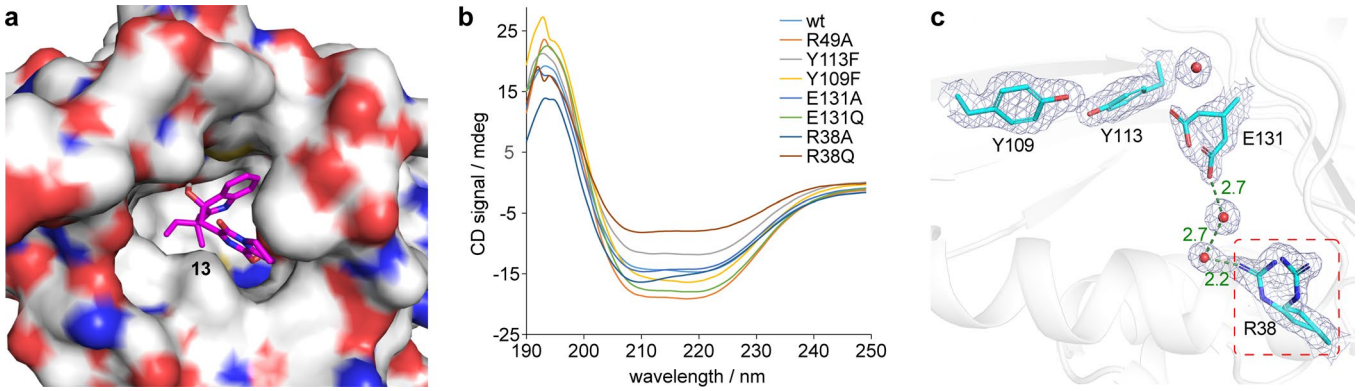

Extended Data Fig. 6 | Docking results and CD spectra of BvnE. a, Docking complex of BvnE with compound **13** (magenta). **b**, CD spectra of purified wild-type and mutant BvnE proteins. **c**, Electron density ($2F_o$-F_c, 1σ) for the active site residues of BvnE (PDB ID code: 6U9I) shows conformational flexibility at Arg38 and Glu131 suggestive of potential active site remodeling during catalysis. Arg38 (red box) which is essential for catalytic activity does not make direct interactions with the docked ligand or active site residues. However, the structure reveals two ordered water molecules (red spheres) in a hydrogen bonding network between Arg38 and Glu131. These binding poses reveal possible key interactions between the ligand and BvnE.

nature research

Corresponding author(s): Robert M. Williams, David H. Sherman, Shengying Li

Last updated by author(s): Feb 18, 2020

Reporting Summary

Nature Research wishes to improve the reproducibility of the work that we publish. This form provides structure for consistency and transparency in reporting. For further information on Nature Research policies, see Authors & Referees and the Editorial Policy Checklist.

Statistics

For all statistical analyses, confirm that the following items are present in the figure legend, table legend, main text, or Methods section.

n/a	Confirmed
☐	☒ The exact sample size (*n*) for each experimental group/condition, given as a discrete number and unit of measurement
☐	☒ A statement on whether measurements were taken from distinct samples or whether the same sample was measured repeatedly
☒	☐ The statistical test(s) used AND whether they are one- or two-sided *Only common tests should be described solely by name; describe more complex techniques in the Methods section.*
☒	☐ A description of all covariates tested
☒	☐ A description of any assumptions or corrections, such as tests of normality and adjustment for multiple comparisons
☒	☐ A full description of the statistical parameters including central tendency (e.g. means) or other basic estimates (e.g. regression coefficient) AND variation (e.g. standard deviation) or associated estimates of uncertainty (e.g. confidence intervals)
☒	☐ For null hypothesis testing, the test statistic (e.g. *F*, *t*, *r*) with confidence intervals, effect sizes, degrees of freedom and *P* value noted *Give P values as exact values whenever suitable.*
☒	☐ For Bayesian analysis, information on the choice of priors and Markov chain Monte Carlo settings
☒	☐ For hierarchical and complex designs, identification of the appropriate level for tests and full reporting of outcomes
☒	☐ Estimates of effect sizes (e.g. Cohen's *d*, Pearson's *r*), indicating how they were calculated

Our web collection on statistics for biologists contains articles on many of the points above.

Software and code

Policy information about availability of computer code

Data collection	XDS
Data analysis	Phenix, Coot, , PyMOL, MolProbity, Autodock4, Phaser-MR, ORCA 4.0, GoodVibes 2.0.3, Gaussian 16, NBO 6.0, Bruker SHELXTL (version 2018/3), CrysAlisPro

For manuscripts utilizing custom algorithms or software that are central to the research but not yet described in published literature, software must be made available to editors/reviewers. We strongly encourage code deposition in a community repository (e.g. GitHub). See the Nature Research guidelines for submitting code & software for further information.

Data

Policy information about availability of data

All manuscripts must include a data availability statement. This statement should provide the following information, where applicable:

- Accession codes, unique identifiers, or web links for publicly available datasets
- A list of figures that have associated raw data
- A description of any restrictions on data availability

Coordinates and associated structure factors have been deposited in Protein Data Bank (PDB) with the PDB ID 6U9I (BvnE) and in the Cambridge Crystallographic Data Centre (CCDC) with the CCDC numbers 1973959 (BX), 1973957 (BY), and 1973958 (15). Sequence data referenced in this study are available in GenBank with the accession number MN401751.

Field-specific reporting

Please select the one below that is the best fit for your research. If you are not sure, read the appropriate sections before making your selection.

☒ Life sciences ☐ Behavioural & social sciences ☐ Ecological, evolutionary & environmental sciences

For a reference copy of the document with all sections, see nature.com/documents/nr-reporting-summary-flat.pdf

Life sciences study design

All studies must disclose on these points even when the disclosure is negative.

Sample size	For X-ray structures, sample size (total number of reflections) was determined by examining % completeness, multiplicity, and Rmerge. This typically amounted to a 360 degree rotation of a single crystal during X-ray data collection. No datasets were reported from multiple crystals. Resolution cutoffs were determined by examining I/sigma, CC1/2, and Rmerge. A thorough conformational analysis (automated with a python script for ground states and performed manually for transition states) was carried out in all the reaction steps studied computationally. Enzymatic assays were performed in triplicate.
Data exclusions	Some reflections are automatically rejected during X-ray data processing and scaling. Default rejection criteria were used in the data processing software (XDS). 5-10% of unique reflections were randomly excluded (Free-R).
Replication	All attempts at replication were successful. It should be noted that each crystal structure reported in this work was determined from a single crystal.
Randomization	Free-R flag for crystallographic data was assigned randomly to unique reflections using CCP4 program Freerflag or Phenix.
Blinding	Not applicable.

Reporting for specific materials, systems and methods

We require information from authors about some types of materials, experimental systems and methods used in many studies. Here, indicate whether each material, system or method listed is relevant to your study. If you are not sure if a list item applies to your research, read the appropriate section before selecting a response.

Materials & experimental systems

n/a	Involved in the study
☒	☐ Antibodies
☐	☒ Eukaryotic cell lines
☒	☐ Palaeontology
☒	☐ Animals and other organisms
☒	☐ Human research participants
☒	☐ Clinical data

Methods

n/a	Involved in the study
☒	☐ ChIP-seq
☒	☐ Flow cytometry
☒	☐ MRI-based neuroimaging

Eukaryotic cell lines

Policy information about cell lines

Cell line source(s)	NRRL (Penicillium brevicompactum) & Gift from Prof. Oikawa laboratory (Aspergillus oryzae)
Authentication	Genome sequencing (Penicillium brevicompactum) & nutritional deficienty traits (Aspergillus oryzae)
Mycoplasma contamination	Negative
Commonly misidentified lines (See ICLAC register)	N/A